ELSEVIER

Journal of Membrane Science 158 (1999) 277–288

journal of MEMBRANE SCIENCE

Hydrophobic silica membranes for gas separation

Renate M. de Vos[*,a], Wilhelm F. Maier[b,1], Henk Verweij[a]

[a] *University of Twente, Faculty of Chemical Technology, Laboratory of Inorganic Materials Science, P.O. Box 217, 7500 AE, Enschede, The Netherlands*

[b] *Max Planck Institut für Kohlenforschung, Kaiser-Wilhelm-Platz 1, D-45470, Mülheim an der Ruhr, Germany*

Received 14 October 1998; received in revised form 14 January 1999; accepted 14 January 1999

Abstract

The synthesis and properties of hydrophobic silica membranes are described. These membranes show very high gas permeance for small molecules, such as H_2, CO_2, N_2, O_2, and CH_4, and permselectivities of 20–50 for these gases with respect to SF_6 and larger alkanes like C_3H_8 and *i*-C_4H_{10}. The membranes are prepared by repeated dip coating of supported γ-alumina membranes in a silica sol solution, followed by drying and calcining. The hydrophobic nature of the membranes is obtained by adding methyl-tri-ethoxy-silane (MTES) to the sol prepared by acid-catalysed hydrolysis and condensation of tetra-ethyl-ortho-silicate (TEOS). The double silica membrane layer has a total thickness of 60 nm and a pore Ø of ca. 0.7 nm. The membranes are 10× more hydrophobic than the state-of-the-art silica membranes which makes them more suitable for application in humid process streams. Besides that, the very high permeance obtained for N_2 and O_2 of 4 and 7×10^{-7} mol/m^2 s Pa, respectively, offer perspectives on dedicated air purification in which larger impurity molecules are blocked by molecular sieving effects.

Keywords: Ceramic membranes; Gas separations; Hydrophobic membranes; Membrane preparation and structure; Microporous and porous membranes

1. Introduction

Silica membranes have been known for about a decade [1]. They can be used in many applications such as gas separation, liquid separation and pervaporation [2–5]. State-of-the-art microporous silica membranes have good gas separation properties [2] but suffer from water sorption sensitivity at room temperature due to the hydrophilic nature of the silica surface. Sorption of moisture, for instance from air, can result in pore blocking with a large impact on separation properties. Interaction of the membrane with water from process streams at higher temperatures can result in serious degradation phenomena [6,7]. Hence, it is important to make the internal (pore) surfaces of the silica material more hydrophobic because:

- It can be expected that this will seriously affect water vapour adsorption and transport
- This enables us to study the effect of hydrophobicity on membrane degradation

*Corresponding author. Tel.: +31-53-430-1408; fax: +31-53-489-4124; e-mail: h.verweij@ct.utwente.nl

[1]Tel.: +49-208-306-2447; fax: +49-208-306-2987; e-mail: maier@mpi-muelheim.mpg.de

0376-7388/99/$ – see front matter
PII: S0376-7388(99)00035-6

- It can be expected that this will affect the transport properties of all polar small molecules

Interaction of water molecules with silica surfaces depends on the presence of functional surface groups. For silica surfaces hydroxyl groups are the most active sites for interaction with water molecules, so the concentration and nature of these groups largely determines the extent of water–membrane interaction [8]. Increasing the hydrophobicity is usually done by elimination of surface hydroxyl groups by:

- chemical modifications such as surface treatments with various alkylsilanes; and
- thermal treatment.

Direct modification of the internal (pore) surface with alkyl- or chlorosilanes is only possible if these compounds can enter the porous structure, so this method can only be used for mesoporous systems and not for microporous membranes [9]. The chloride ion, however, is small enough to enter the micropores and can be exchanged with the surface hydroxyls. Unfortunately, this process is reversible so that Si–Cl bonds will be transformed back into Si–OH bonds if the surface comes in contact with water molecules [10]. Thermal treatment at ca. 800°C can be quite effective since it removes almost all surface hydroxyls, and the subsequent rehydroxylation is very slow compared to materials that can be dehydroxylated at lower temperatures [8]. A temperature of 800°C, on the other hand, results in sintering of the silica structure to almost full density. Therefore, the percolative micropore structure, needed for the special separation properties, is lost. Hence, thermal dehydroxylation cannot be used for our microporous silica membranes.

In the present study, we propose an alternative method for decreasing water molecule interaction or, in other words, increasing *hydrophobicity* by adapting the synthesis of the sol solution. The properties of hydrophobic aerogels and silica glass surfaces have been reported before in [11–16] but, to our knowledge, this is the first paper that describes the properties of calcined hydrophobic silica membranes in gas separation experiments. The present study provides initial results on the synthesis, surface and transport properties of hydrophobic silica membranes together with a comparison of these aspects with 'standard' silica membranes.

2. Experimental

The microporous membranes were applied on top of γ-alumina membranes carried by porous α-alumina discs. These discs had a Ø of 39 and 2 mm thickness, a porosity of 40% and an average pore size of 160 nm. The γ-alumina membranes were 3–5 μm thick and had a porosity of ~40%, and an average cylindrical pore radius of 2.5 nm. All membrane preparation was performed under class 100 clean room conditions to avoid the formation of meso- and macroscopic defects in the microporous membrane structure. Such defects are expected to have a negative influence on over–all membrane selectivity and membrane lifetime properties.

2.1. Standard silica membrane preparation

'Standard' (hydrophilic) silica membranes, further indicated as 'Si(400) membranes', were prepared for comparison by dip-coating a supported γ-alumina membrane in a diluted sol, followed by thermal treatment. The standard silica sol is prepared by acid-catalysed hydrolysis and condensation of tetra-ethyl-ortho-silicate (TEOS)[2] in ethanol. A mixture of acid and water is carefully added to a mixture of TEOS and ethanol under vigorous stirring followed by 3 h heating at 60°C. The complete preparation procedure is described elsewhere [3].

2.2. Hydrophobic membrane preparation

In order to make the silica membrane material more hydrophobic, methyl-tri-ethoxy-silane (MTES)[3] is incorporated at a certain stage of sol preparation. The hydrolysis/condensation rate at room temperature of MTES is ~7 times higher than that of TEOS [17]. This implies that the reaction time of MTES should be ~7 times shorter to obtain silica polymers with dimensions similar to those obtained with hydrolysis and condensation of TEOS. This simple consideration led us to the idea to start with a 'standard' silica sol solution preparation and add MTES after 6/7 of the normal total reaction time at least. If MTES was added earlier, for instance after 2/3 of the total reaction time,

[2] p.a. grade, Aldrich Chemical, Milwaukee, WI, USA.
[3] Same as in footnote 1.

more 'bulky' polymers were formed, visible through light scattering in the sol solution. This implied that, in that case, the polymer particles formed had dimensions >10 nm, which would hamper the formation of a microporous membrane structure in later stages of the process.

The complete sol preparation procedure for hydrophobic membranes was as follows: TEOS was mixed with ethanol and placed in an ice bath to avoid premature (partial) hydrolysis. A mixture of acid and water was added under vigorous stirring. After addition, the reaction mixture was heated for $2\frac{3}{4}$ h at 60°C in a water bath under continuous stirring. The reaction mixture had a molar ratio (based on unreacted components) TEOS/ethanol/water/acid of 1/3.8/6.4/0.085 according to the 'standard' recipe of silica sol preparation, as presented in [18]. MTES was mixed with ethanol in the ratio of 1 : 3.8 and placed in an ice bath. This mixture was added to the TEOS reaction mixture that was refluxed $2\frac{3}{4}$ h and the MTES/TEOS reaction mixture obtained was heated for another 15 min at 60°C. The mixture then had a molar ratio MTES/TEOS/ethanol/water/acid (based on unreacted components) of 1/1/7.6/6.4/0.085. Subsequently, the reacted mixture was cooled and diluted 19-fold with ethanol to obtain the final dip-coating solution. After dip coating, the membranes were calcined at 400°C for 3 h in pure N_2 using a heating and cooling rate of 0.5°C/min. Some active carbon pellets[4] were placed in the vicinity of the membranes to capture traces of oxygen in the N_2 stream. Calcination was done in N_2 (instead of air for the standard membranes) to avoid premature oxidation of the CH_3 groups. The whole process of dipping and calcining was repeated once to repair any defects in the first silica membrane layer. The membranes obtained in this way are henceforth referred to as 'MeSi(400) membranes'.

2.3. Unsupported silica materials

Unsupported microporous silica materials were made for characterisation by means of physical adsorption measurements as follows: 60 cm^3 of 19× ethanol—diluted, hydrolysed silica sol, prepared as described before, was allowed to evaporate in a 10-cm Ø Petri-dish at room temperature, so that 0.1–0.3 mm thick silica gel flakes were obtained overnight. This was done for both 'standard' sols and sols to which MTES was added. The calcination procedure was the same as for the supported membranes. In addition, samples were taken from sols prepared with MTES/TEOS as described before, but with deviating MTES hydrolysis times of 5, 10, and 20 min. This was done to describe the characteristics of the material at several stages of the hydrophobic sol synthesis. These samples were treated as described above.

2.4. Membrane characterisation

Morphological characterisation of supported hydrophobic silica membranes was done by field-emission scanning electron microscopy (FE-SEM)[5] of a perpendicular membrane cross section. The presence of methyl groups in the microporous structure was demonstrated with IR (FTIR) spectroscopy.[6] For that purpose, a KBr pellet was made of 20 mg unsupported material and 200 mg KBr. The pellet was heated in a pure Ar stream in an IR-cell[7] with KBr windows at 400°C for 20 h to remove water and weakly bound surface hydroxyls. The spectra were recorded at 30°C (200 Scans) in the diffuse reflectance mode and represented by application of the Kubelka–Munk function [19].

The hydrophobicity of the unsupported membrane material is determined by measuring the hydrophobicity index $HI = x_{octane}/x_{water}$ as described in [20,21]. For that purpose, the sample was dried for 12 h at 250°C in a pure Ar stream. After that an Ar stream containing defined and equal concentrations of water and octane was used to load the sample to saturation at a temperature of 30°C. The Ar, water and octane flow rates were controlled by mass flow meters. The breakthrough curves of the individual components were obtained by on-line gas chromatography. Numerical integration of the normalised breakthrough curves

[4]Norit RGM 0.8, Quality A3687, Norit N.V., Amersfoort, The Netherlands.

[5]Hitachi, Type S800.

[6]IFS 46, Bruker, Ettlingen, Germany.

[7]HVC/diffuse reflectance unit DRA-XX, Harrick Scientific Corporation, Ossining, NY.

provided the sample loading of water, x_{water}, and octane, x_{octane}. These values were corrected for background signals originating from the reactor. An impression of the difference in hydrophobicity of the membranes could also be obtained directly by putting a drop of water on both the membrane types and observing the difference in curvature of the drops.

Thermogravimetric analysis (TGA)[8] was performed on unsupported material to get a qualitative indication of the amount of hydroxyl groups at the surface. The TGA samples were stored in laboratory air at room temperature and, hence, at normal relative humidity before measurement. Unsupported material, made from the standard dipping solution (Si(400)) but not calcined, was examined by TGA as well to determine the burnout of the organic groups. The TGA experiments were performed with a heating rate of 1°C/min to 800°C in a pure N_2 stream and with a water and oxygen content <5 ppm.

Adsorption isotherms were determined by both Ar and N_2 sorption, since it is expected that Ar shows no specific interactions with the surface, while N_2 is expected to show particular interaction with the hydroxyl groups at the surface and might, therefore, be sorbed more on Si(400) [8,22]. Ar adsorption was performed at both, liquid N_2 and Ar temperature (77 and 87 K, respectively). The physical gas adsorption set-up[9] was provided with a turbo molecular pump system[10] and an extra pressure transducer for the low-pressure range (10^{-3}–10 Torr). The latter was needed for measuring microporous adsorption, which was checked by measuring zeolites silicalite, 13X and 5A [23].

Single-gas permeance experiments of the membranes were performed with a dead-end set-up [24], a detailed description of which is given elsewhere [3]. Prior to the permeance experiments, the membranes were dried at 300°C under an He stream to remove any moisture from the pore structure of the support, the γ-alumina intermediate layer and the silica top-layer. All characterisations were done for both, Si(400) and MeSi(400).

[8]Type 1136, Setaram, Lyon, France.
[9]Sorptomatic 1990, Carlo Erba Instruments, Milan, Italy.
[10]Turbotronik, NT50 Leybold, Hanau, Germany.

3. Results and discussion

3.1. Morphological characterisation of hydrophobic silica membranes

FE-SEM micrographs are shown in Fig. 1(A and B). In Fig. 1(A), a cross section of the whole membrane is visible. In the lower right corner, the α-alumina support is visible with two γ-alumina layers (~2 μm thick) on top. The two silica layers in the upper left hand corner are barely perceptible. Fig. 1(B) depicts a magnification of the surface part of the cross section in which two separate silica layers are clearly visible; both having a thickness of ca. ~30 nm.

3.2. Infra-red spectroscopy

Fig. 2 depicts the IR-spectra of unsupported Si(400) and MeSi(400) materials. In the methylated material, a sharp extra absorption peak is found around 1280 cm^{-1}. This peak is ascribed to asymmetric deformation vibrations of the CH_3 groups [25].

3.3. Hydrophobicity

Measurement of breakthrough curves of water and octane resulted in $HI = 0.3$ for the unsupported Si(400) material and $HI = 3.0$ for the MeSi(400) material. The methylated unsupported membrane material is thus very hydrophobic while the standard silica material is strongly hydrophillic. The value of $HI = 3.0$ for amorphous microporous silica is similar to a value of $HI = 2.9$ found by Maier et al. for a methylated silica–titania hybrid material [20]. For zeolites, however, higher values are measured, such as $HI = 10.3$ for silicalite I [21] which offers perspectives for further improvement of our silica material.

As can be seen in Fig. 3 a water drop becomes more spread out on top of a Si(400) membrane than on a MeSi(400) membrane. This confirms that the MeSi(400) membranes are more hydrophobic than the Si(400) membranes.

3.4. Thermogravimetric analysis

The thermogravimetric experiments demonstrated a clear difference between the thermochemical proper-

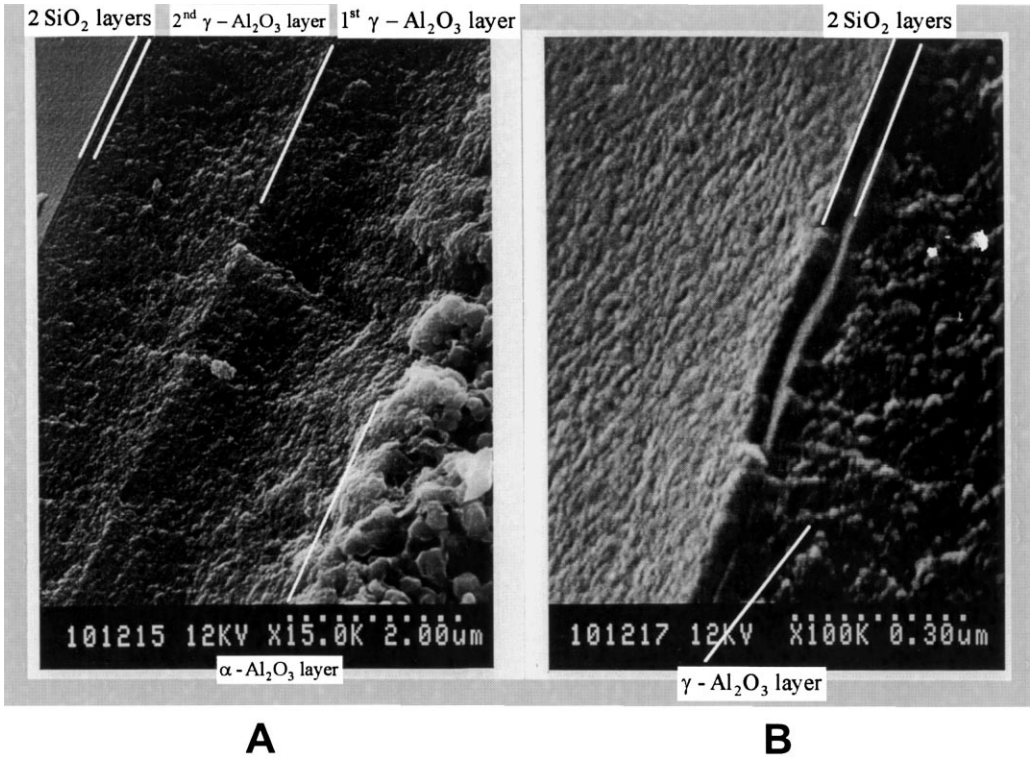

Fig. 1. FE-SEM micrographs of MeSi(400) cross sections.

ties of Si(400) and MeSi(400) materials (see Fig. 4). The MeSi(400) material does not show any weight loss up to 500°C, while the Si(400) material already starts to lose weight below 100°C. This low-T weight loss of Si(400) is ascribed, as usual, to evaporation of physisorbed water [8,26]. The lack of such a low-temperature weight loss for the MeSi(400) material indicates that in this material water sorption from ambient air hardly occurs. The total weight loss of both materials is quite different as well. Si(400) shows a weight loss of ca. 2%, caused by the loss of adsorbed water and surface hydroxyls at elevated temperatures. MeSi(400) shows a weight loss starting at much higher

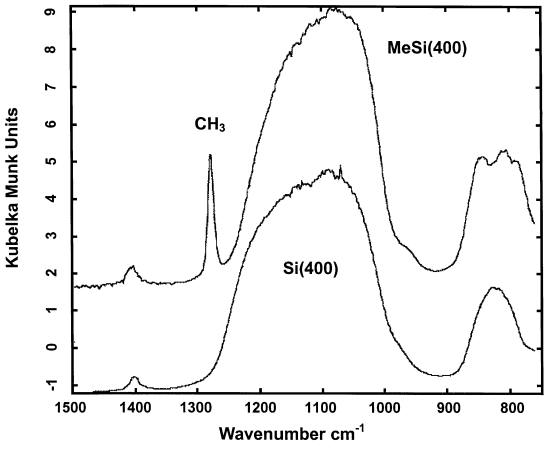

Fig. 2. IR KBr pellet spectra of unsupported MeSi(400) and Si(400) material.

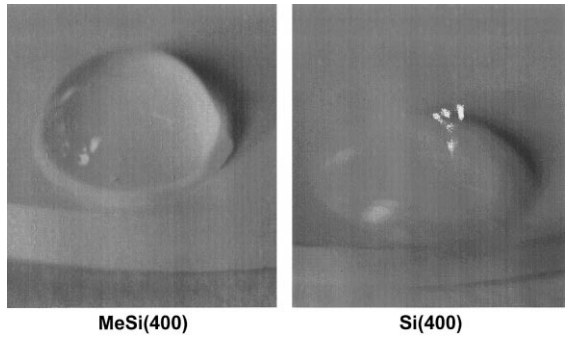

Fig. 3. Drop of water on MeSi(400) and Si(400) membrane.

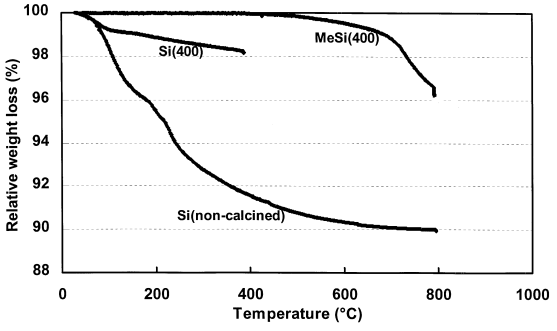

Fig. 4. TGA, relative weight loss vs. T for MeSi(400), Si(400) and non-calcined Si material.

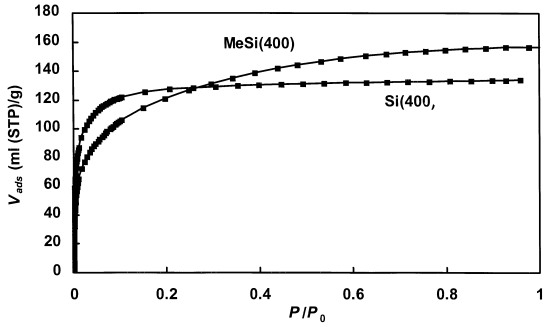

Fig. 5. N_2 adsorption isotherm at 77 K of unsupported MeSi(400) and Si(400) material; $P_0 = 101.3$ kPa.

temperatures that saturates at 4% around 800°C. Hence, MeSi(400) is concluded to be thermochemically stable until ~500°C in pure N_2. The weight loss of MeSi(400) in N_2 at higher temperatures might be due to the loss of incorporated methyl groups with the formation of CH_4 or H_2. Theoretically, a weight loss of 12% is expected if all methyl groups, that are initially introduced in the synthesis, are removed in this way. It was found that after the TGA experiments the MeSi(400) material had turned black while the Si(400) material remained white. This led us to the conclusion that, after the TGA run, not all carbon atoms of the CH_3 groups were removed from the MeSi(400) material and it is likely that thermally induced condensation of methyl groups had occurred in a reaction such as:

(1)

If, for instance, every two methyl groups combine, as happens in reaction (1), a maximum weight loss of 6.4% is expected. The fact that the actual weight loss observed is $\ll$6.4% can be explained as follows:

- The relatively low concentration of methyl groups makes it unlikely that all methyl groups can participate in a reaction such as (1).
- It is unlikely that all methyl groups initially added during synthesis, are actually incorporated in the calcined material.
- The actual condensation mechanism is not clear yet and the formation of, for instance –CH_2– groups, has never been found up to now.

3.5. Analysis of sorption data

Gas adsorption isotherms were determined with both, Ar and N_2 for unsupported MeSi(400) and Si(400). It was observed that, at 77 K, slightly more Ar was adsorbed than at 87 K. For the sake of clarity, only the 77 K isotherms are depicted in Figs. 5 and 6. The differences between interactions of the material surface with the sorbent are very clear from a comparison of Figs. 5 and 6. Taking into account the molecular dimensions of the gas molecules, it can be expected that more Ar can be adsorbed than N_2: Ar has a kinetic diameter, d_k, of 0.340 nm and covers a sorption area of 0.133 nm^2, while N_2 has a d_k of 0.365 nm and covers a sorption area of 0.166 nm^2 [8]. For MeSi(400) material, it is observed indeed that more Ar can be adsorbed than N_2. For Si(400), however, the amount of N_2 that can be adsorbed is larger than that of Ar. This implies that in the adsorption on

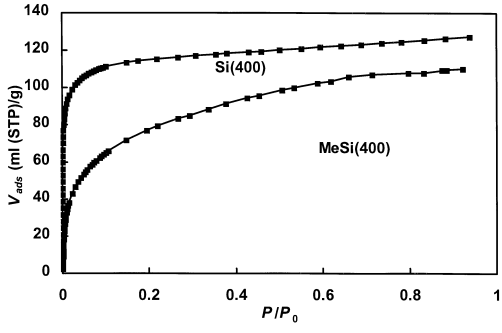

Fig. 6. Ar adsorption isotherm at 77 K of unsupported MeSi(400) and Si(400) material; $P_0 = 26.7$ kPa.

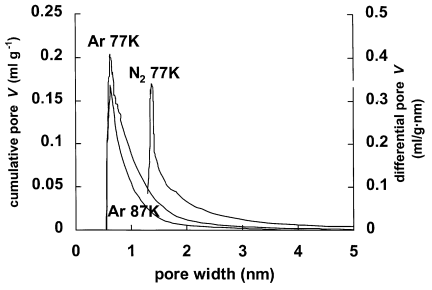

Fig. 7. Pore volume (V) vs. size distribution for unsupported Si(400) material, calculated according to the Horváth–Kawazoe method [28] from adsorption isotherms for gasses and temperatures as indicated.

Si(400), specific surface interactions are involved that influence the amount of gas that can be adsorbed.

The difference between Ar and N_2 adsorption becomes even more pronounced if the Horváth–Kawazoe pore size distribution is calculated from the isotherms [28]. The average pore size of the Si(400) material that can be calculated from the N_2 isotherm is almost twice as large as that obtained from the Ar isotherm (see Fig. 7). Since the Ar molecule is spherical and more 'inert' than the N_2 molecule,[11] it is assumed that the calculation based on the Ar isotherm approaches the real pore geometry situation best [27]. This is supported by the gas permeation results, to be discussed in Section 3.6. In Table 1 the total adsorbed amount, V_{ads}, the surface area, SA, and the pore diameter, d_p, according to Horváth–Kawazoe [28] are given for unsupported Si(400) and MeSi(400) samples in different stages of the sol preparation. For all hydrophobic (MeSi) samples $V_{ads}(Ar) \geq V_{ads}(N_2)$; $SA(N_2)$ shows a tendency of slight decrease with hydrolysis time while SA(Ar) remains approximately constant with hydrolysis time. Since N_2 is assumed to show particular affinity for hydroxyl groups [22], this observation led us to the tentative conclusion that in samples with an increasing MTES hydrolysis time, the pore structure remains constant while the amount of OH-groups decreases. This is to be expected, since every Me–Si group replaces formally a surface HO–Si group. The shape of the isotherm and of the calculated pore size distribution

[11]Besides the hydroxyl interactions already mentioned, the interpretation of N_2 adsorption data is further complicated by quadrupolar interactions.

Table 1
V_{ads}, SA and d_p of Si(400) and MeSi(400) samples after 5, 10, 15 and 20 min hydrolysis

Sample	V_{ads} (ml (STP)/g)		SA (m^2/g)		d_p (nm)	
	N_2	Ar	N_2	Ar	N_2	Ar
Si(400)	155	145	498	432	1.4	0.62
MeSi 5 min	150	175	417	413	1.4	0.67
MeSi 10 min	125	130	408	409	1.7	0.7
MeSi 15 min	110	150	341	413	>2.0	0.7
MeSi 20 min	100	120	382	399	1.7	0.73

of Fig. 8, however, indicate that MeSi(400) has a broader pore size distribution than Si(400).

3.6. Gas permeance

Prior to the gas permeance experiments, the membranes were dried in an He stream at 300°C until the He flux was stable. For Si(400) membranes such a process can easily take 3–4 h. For MeSi(400) membranes, this process required only 30 min, consistent in part with the TGA analysis of the MeSi(400) material that did not reveal any weight loss and, hence, release of adsorbed water, up to a temperature of 500°C. The fact that some stabilisation time is still needed indicates that water adsorbed in the supported MeSi(400) membranes is likely to be present in the γ-alumina layer only, which is still rather hydrophilic. The above assumption is supported by a calculation using the Kelvin relation (Eq. (2)) of the relative water pressure, P_{rel}, at which capillary condensation of water in the pores of the γ-alumina layer

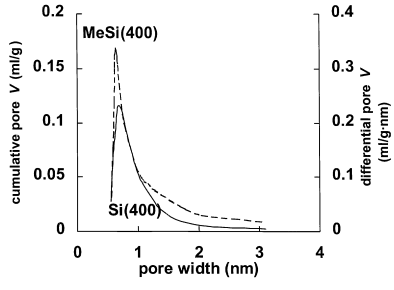

Fig. 8. Pore volume (V) vs. size distribution for unsupported MeSi(400) and Si(400) material, calculated according to the Horváth–Kawazoe method [28] from Ar adsorption isotherms at 87 K.

will occur:

$$\ln P_{\mathrm{rel}} = -\frac{2\gamma_s V_{\mathrm{mol}}}{RT}\frac{1}{r_K} \quad (2)$$

Here, γ_s is the surface tension (at 20°C) of the water/vapour interface, V_{mol} the molar volume of (condensed) water, R the gas constant, T the absolute temperature and r_K the Kelvin radius. To obtain a rough estimate, r_k can be taken equal to 2.5 nm assuming a contact angle of 0° and a '*t*-layer' [29] of negligible thickness. This leads, with $\gamma_s = 7.28 \times 10^{-2}$ N/m, to the occurrence of capillary condensation of water in the γ-alumina pores at 20°C and relative humidity of 65%. Hence, if we take the presence of a *t*-layer into account, we may safely assume that under normal laboratory circumstances the γ-alumina pores will be filled with water. This means that for freshly prepared MeSi(400) membranes some time is still needed before the absorbed water in the γ-Al_2O_3 pores is evaporated in the dry permeation cell environment and the permeation flux becomes stationary. This process, however, takes much less time than the evaporation of water molecules from the micropores in Si(400).

Permeance, F, data at different P and T, not corrected for support resistance, are given in Table 2. From this table, it is clear that the F for most gasses shows a T-dependence like that of Knudsen diffusion: slightly increasing F with decreasing T. At first sight this suggests that the membranes are mesoporous. On the other hand, SF_6 ($d_k = 0.55$ nm) and i-C_4H_{10} ($d_k = 0.5$ nm) hardly permeate through the MeSi(400) membranes, $F(SF_6)$ is found to be $\sim 1 \times 10^{-9}$ mol/m^2 s Pa, so that the maximum pore size of the membranes is expected to be ~0.55 nm.

The microporous nature of the membranes can be perceived from the permselectivity, F_α, data that can be derived from Table 2. $F_\alpha(H_2/CO_2) = 6$; $F_\alpha(H_2/N_2) \cong F_\alpha(H_2/CH_4) \cong 8$ and $F_\alpha(H_2/i\text{-}C_4H_{10})$ is >300. Evidently, the F_α's exceed the Knudsen separation value which is, in most cases, of the order of unity. As a consequence, the 'Knudsen like' T-dependence observed for F is likely to be caused by the support,[12] which has a large influence, especially for H_2, on the total F through the composite membrane structure: $F(H_2)$ for an MeSi(400) membrane is only 25% lower than F(support) under the same conditions. Hence, the support resistance should not be ignored since it might even dominate transport properties.

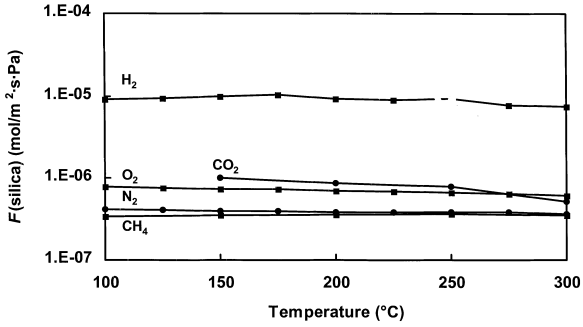

Fig. 9. MeSi(400) membrane F vs. T, corrected for support resistance, for several gasses at $\Delta P = 1.5$ bar.

The permeance, F(silica), of the silica membrane layer may be obtained from the overall permeance, F, and the support permeance, F(silica), by the application of:

$$\frac{1}{F} = \frac{1}{F(\mathrm{support})} + \frac{1}{F(\mathrm{silica})} \quad (3)$$

F(support), measured at relevant T and P, is given in Table 3 and used for the calculation of F(silica) in Fig. 9 and F_α(silica) in Fig. 10. F(support) was found to be P-independent for all gasses, which indicates that the transport through the γ-alumina membranes was mainly in the Knudsen regime. The latter conclusion is supported by the fact that, for the F-values of Table 3, the product $F \times \sqrt{T} \times \sqrt{M}$, in which M is the molar mass of the gas molecules, shows little variation. For molecules larger than CH_4, corrections

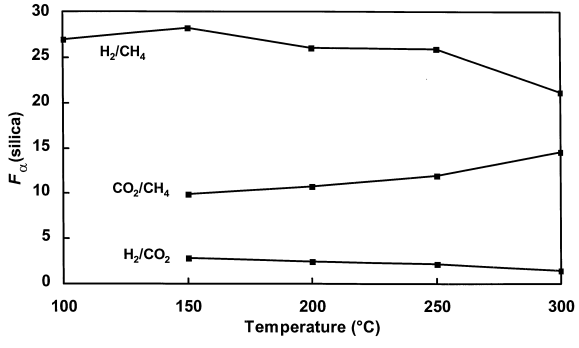

Fig. 10. MeSi(400) membrane F_α vs. T, corrected for support resistance, for several gasses at $\Delta P = 1.5$ bar.

[12] Supported γ-alumina membrane without silica layer.

Table 2
MeSi(400) membrane F, not corrected for support resistance with a permeate $P = 1$ bar

Gas	ΔP [bar]	$F \times 10^7$ (mol/m^2 s Pa) at:								
		100°C	125°C	150°C	175°C	200°C	225°C	250°C	275°C	300°C
H_2	0.5	22.2	22.7	21.6	21.3	20.6	20.3	20.1	19.6	18.6
	1.0	22.7	22.4	22.2	21.8	20.9	20.5	20.4	19.5	19.1
	1.5	24.0	23.6	23.3	23.1	22.0	21.4	21.2	19.9	19.4
	2.0	24.3	24.2	23.7	23.3	22.3	21.8	21.6	20.4 [a]	
He	0.5	13.3	13.0	12.7	12.9	12.6	12.6	12.5	12.1	12.7
	1.0	12.7	13.0	12.8	12.8	12.7	12.6	12.5	12.3	11.9
	1.5	13.0	12.9	13.0	12.9	12.7	12.7	12.4	12.3	11.9
	2.0	13.0	13.2	13.2	13.1	13.0	12.8	12.7	12.5	12.2
	2.5	13.2	13.4	13.4	13.3	13.3	13.1	12.9	12.6	12.3
	3	13.5	13.5	13.5	13.5	13.4	13.3	13.1	12.8	12.5
CO_2	0.5	4.84	4.62	4.33	4.21	3.80	3.58	3.29	3.02	2.71
	1.0	5.05	4.78	4.54	4.30	4.14	3.82	3.65	3.31	2.97
	1.5	5.15	4.92	4.73	4.44	4.11	3.88	3.67	3.40	3.08
	2.0	5.18	4.89	4.64	4.47	4.05	3.91	3.73	3.47	3.14
	2.5	5.35	5.09	4.78	4.48	4.12	3.8	3.47	3.16	2.83
	3	5.53	5.22	4.96	4.64	4.31	3.98	3.66	3.39	2.82
O_2	0.5	3.79	3.66	3.43	3.45	3.23	3.28	3.15	3.01	2.88
	1.0	3.89	3.78	3.68	3.61	3.54	3.40	3.35	3.25	3.11
	1.5	4.09	3.95	3.85	3.79	3.63	3.58	3.47	3.36	3.23
	2.0	4.15	4.05	3.97	3.84	3.76	3.67	3.54	3.44	3.35
	2.5	4.26	4.16	4.05	3.95	3.84	3.72	3.62	3.51	3.39
	3		4.13	4.12	3.96	3.86	3.76	3.67	3.61	3.46
N_2	0.5	2.52	2.46	2.43	2.41	2.33	2.28	2.25	2.27	2.11
	1.0	2.75	2.68	2.61	2.62	2.55	2.48	2.44	2.4	2.34
	1.5	2.87	2.80	2.72	2.68	2.61	2.57	2.56	2.53	2.45
	2.0	2.94	2.87	2.79	2.75	2.67	2.67	2.62	2.61	2.53
	2.5	2.97	2.90	2.84	2.8	2.71	2.69	2.67	2.63	2.55
	3	3.03	2.97	2.90	2.85	2.77	2.75	2.7	2.67	2.63
CH_4	0.5	2.64		2.64		2.64		2.56		2.6
	1.0	2.66		2.68		2.68		2.66		2.63
	1.5	2.69		2.71		2.71		2.7		2.63
	2.0	2.69		2.71		2.71		2.71		2.68
	2.5	2.66		2.66		2.66		2.69		2.62
	3	2.58		2.65		2.65		2.63		2.48
C_3H_8	1	0.0722		0.149		0.101		0.083		0.0505
	1.25	0.202		0.197		0.137		0.119		0.0751
	1.5	0.197		0.192		0.147		0.121		0.0818
	1.75	0.205		0.194		0.147		0.130		0.0907
i-C_4H_{10}	1			0.0429		0.0443		0.0403		0.0356
	1.25			0.088		0.0451		0.0467		0.0494
	1.35			0.103		0.0557		0.0576		0.0497
	1.5			0.0966		0.0662		0.0685		0.0508

[a] From this ΔP and T onwards, the H_2 flux exceeded the maximum possible value of our set-up.

Table 3
F(support) data used for support resistance correction calculations

Gas	$F \times 10^7$ (mol/m^2 s Pa) at								
	100°C	125°C	150°C	175°C	200°C	225°C	250°C	275°C	300°C
H_2	32.5	31.4	30.5	29.6	28.8	28.1	27.4	26.8	26.2
CO_2			8.97		7.86		6.91		6.25
N_2	9.26	8.97	8.70	8.45	8.22	8.02	7.82	7.64	7.47
O_2	8.60	8.32	8.07	7.84	7.63	7.44	7.26	7.09	6.94
CH_4	12.8	12.3	12.0	11.6	11.3	11.0	10.8	10.5	10.3

for support resistance are not performed since, in those cases, the effect of support resistance on *F*(silica) is negligible.

For the smaller gas molecules, the effect of support correction is considerable: as can be seen in Table 3 and Fig. 9, F(H_2, silica) appears to be twice as high as *F*(support); the membrane is in this case more permeable than the support. $F_\alpha(H_2/CO_2,\ \text{silica}) = 9\ldots15$ and is more than twice as high as the non-corrected $F_\alpha(H_2/CO_2)$; for H_2/N_2 and H_2/CH_4 an increase to $F_\alpha(\text{silica}) \cong 22$ is found. F_α(silica) for separation of H_2 from alkanes (>CH_4) becomes even >500 or >1000, depending on the chain length of the alkane. All F_α(silica) values are larger than F_α(Knudsen); even $F_\alpha(O_2/N_2,\ \text{silica})$ becomes ~2 while $F_\alpha(O_2/N_2,\ \text{Knudsen}) = 0.94$. This provides additional evidence that transport in the MeSi(400) membranes is controlled by microporous diffusion and not by Knudsen diffusion.

In Fig. 11, the corrected *F*(silica) is plotted as a function of the d_k. Compared to the Si(400) membranes, the MeSi(400) membranes have larger pores and a larger pore size distribution, which results in a more gradual decrease of *F* with d_k. This is in agreement with Ar adsorption measurements. In Fig. 8, it can be seen that most of the pores in both, Si(400) and MeSi(400) unsupported membrane material have about the same size, but that the amount of larger pores is substantially larger in the MeSi(400) material than in the Si(400) material.

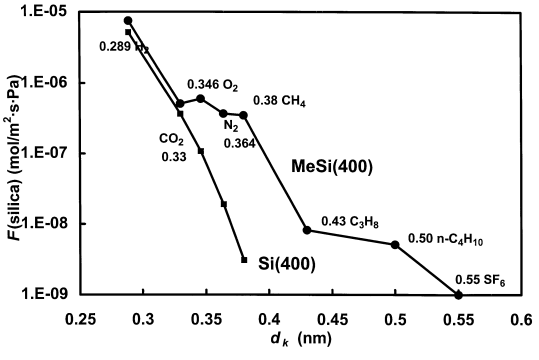

Fig. 11. Si(400) [3] and MeSi(400) membrane *F* vs. d_k of several gasses, corrected for support resistance, at 300°C and $\Delta P = 1.5$ bar.

4. Conclusions

By incorporation of methyl groups in the silica microstructure the surface and microstructural properties of the microporous silica membranes change significantly. The 'MeSi(400) membranes' obtained become 10 × more hydrophobic than state-of-the-art silica 'Si(400) membranes'. Water sorption in MeSi(400) is less compared to that in Si(400) membranes, and only occurs in the support's intermediate γ-alumina layer. This water can be removed easily, however, compared to water that is sorbed in the micropores of Si(400) membranes. MeSi(400) membranes have larger micropores with a wider pore size distribution than Si(400) membranes which influences their transport properties. The MeSi(400) membranes show a 'Knudsen-like' *T*-dependence for *F* of smaller molecules but with an F_α with respect to larger molecules that is considerably higher than the Knudsen values. The 'Knudsen-like' *T*-dependence is likely due to a contribution of the support resistance. By applying a proper correction for support resistance, $F(H_2,\text{silica})$ becomes 1×10^{-5} mol/m^2 s Pa at 250°C which is three times the uncorrected value.

The high *F*-values for small gases such as He, H_2, CO_2, O_2, and N_2, and the diminished adsorption of water molecules, that otherwise block the pores, indicates that MeSi(400) membranes might be suitable for

dedicated air cleaning processes. Another application that becomes attractive with these membranes is the separation of H_2 and other small gases, including CH_4, from higher alkanes in humid process streams.

The objective of the present study was to demonstrate the potential of amorphous hydophobic silica membranes obtained with an exploratory approach. Further development of hydrophobic silica membranes should focus on the following areas:

- Systematic optimisation of the sol–gel and calcination procedures.
- Systematic relation between sol–gel chemistry, pore structure and transport properties.
- Transport studies with gas mixtures that contain water vapour.
- Thinner silica membrane layers to increase permeance.
- Development of more permeable support structures that no longer affect F for smaller molecules.
- Introduction of hydrophobicity on the internal surface by state-of-the-art chemical modification of the γ-alumina intermediate layer and possibly the α-alumina support. This will be necessary in real applications to avoid capillary condensation of water before, and during, the operation in humid process streams.
- Study of the actual water vapour resistance of the membranes at high T and P.

5. List of symbols

γ_s	surface tension (N/m)
d_k	Lennard–Jones kinetic diameter of gas molecules (m)
F	permeance (mol/m^2 s Pa)
F(silica)	membrane permeance, corrected for support permeance (mol/m^2 s Pa)
F(support)	support permeance (mol/m^2 s Pa)
F_α	permselectivity, obtained from single-gas permeation measurements
F_α(silica)	permselectivity, corrected for support permeance
HI	hydrophobicity index, defined in [20,21]
MTES	methyl-tri-ethoxy-silane
P	pressure (Pa)
d_p	pore diameter, obtained by Horváth–Kawazoe analysis [28]
R	gas constant (J/mol K)
SA	specific surface area (m^2/g)
T	absolute temperature (K)
TEOS	tetra-ethyl-ortho-silicate
V_{ads}	specific adsorbed volume (ml (STP)/g)
V_{mol}	molar volume (m^3/mol)

Acknowledgements

The authors are indebted to H. Bretinger, F. Konietzni and Ch. Lange (Max-Planck Institute) for Ar adsorption, IR and hydrophobicity measurements. E.W.J. Römer (University of Twente) is acknowledged for TGA measurements. This project is financially supported by ECN, Petten, The Netherlands.

References

[1] R.J.R. Uhlhorn, M.H.B.J. Huis in't Veld, K. Keizer, A.J. Burggraaf, High permselectivities of microporous silica-modified γ-alumina membranes, J. Mater. Sci. Lett. 8 (1989) 1135.
[2] R.M. de Vos, H. Verweij, High-selectivity, high-flux silica membranes for gas separation, Science 279 (1998) 1710.
[3] R.M. de Vos, H. Verweij, Improved performance of silica membranes for gas separation, J. Membr. Sci. 143 (1998) 37.
[4] A. Larbot, A. Julbe, C. Guizard, L. Cot, Silica membranes by the sol–gel process, J. Membr. Sci. 44 (1989) 289.
[5] R.W. van Gemert, F.P. Cuperus, Ceramic pervaporation membranes for use in high temperature batch processes, in A.L. Zydney (Ed.), Proceedings 9th Ann. meeting, North American Membrane Society, Baltimore, May 31–June 4, F-4, 1997.
[6] H. Imai, H. Morimoto, A. Tominaga, H. Hirashima, Structural changes in sol–gel derived SiO_2 and TiO_2 films by exposure to water vapour, J. Sol-gel Sci. & Techn. 10 (1997) 45.
[7] G.P. Fotou, Y.S. Lin, S.E. Pratsinis, Hydrothermal stability of pure and modified microporous silica membranes, J. Mater. Sci. 30 (1995) 2803.
[8] R.K. Iler, The Chemistry of Silica, Wiley, New York, 1979, Chapter 6.
[9] P. van der Voort, K.C. Vrancken, E.F. Vansant, Gas-phase chlorosilylation of silica gel: effectiveness, surface coverage and stoichiometry, J. Chem. Soc. Faraday Trans. 92 (1995) 353.
[10] M.L. Hair, W. Hertl, Chlorination of silica surfaces, J. Phys. Chem. 77 (1973) 2070.
[11] M. Pauthe, F. Despetis, J. Phalippou, Hydrophobic silica CO_2 aerogels, J. Non-Cryst. Sol. 155 (1993) 110.
[12] H. Yokogawa, M. Yokoyama, Hydrophobic silica aerogels, J. Non-Cryst. Sol. 186 (1995) 23.

[13] C. Della Volpe, S. Dirè, E. Pagani, A comparative analysis of surface structure and surface tension of hybrid silica films, J. Non-Cryst. Sol. 209 (1997) 51.
[14] S. Dirè, E. Pagani, F. Babonneau, R. Ceccato, G. Carturan, Unsupported SiO_2-based organic–inorganic membranes. Part 1. Synthesis and structural characterisation, J. Mater. Chem. 7 (1997) 67.
[15] S. Dirè, E. Pagani, R. Ceccato, G. Carturan, Unsupported SiO_2-based organic-inorganic membranes. Part 2. Surface features and gas permeation, J. Mater. Chem. 7 (1997) 919.
[16] T. Takei, A. Yamazaki, T. Watanabe, M. Chikazawa, Water adsorption properties on porous silica glass surfaces modified by trimethylsilyl groups, J. Coll. Interf. Sci. 188 (1997) 409.
[17] M.J. van Bommel, T.N.M. Bernards, A.H. Boonstra, The influence of the addition of alkyl-substituted ethoxysilane on the hydrolysis-condensation process of TEOS, J. Non-Cryst. Sol. 128 (1991) 231.
[18] R.S.A. de Lange, J.H.A. Hekkink, K. Keizer, A.J. Burggraaf, Formation and characterisation of supported microporous ceramic membranes prepared by sol–gel modification techniques, J. Membr. Sci. 99 (1995) 57.
[19] P. Kubelka, F. Munk, A contribution to the optics of colour coatings (in German), Z. Tech. Phys. 12 (1931) 593.
[20] S. Klein, W.F. Maier, Microporous mixed oxides-catalysts with tunable surface polarity, Angew. Chem. Int. Ed. Engl. 35 (1996) 2230.
[21] J. Weitkamp, P. Kleinschmit, A. Kiss, C.H. Breke, The hydrophobicity index. A valuable test for probing the surface properties of zeolitic adsorbents or catalysts, in R. von Balmoos et al. (Eds.), Proc. 9th Int. Zeolite Conf., Montreal 1992, 1993, pp. 79.
[22] S. Kondo, Colloidal Silicas, in A. Dabrowski, V.A. Tertykh (Eds.), Adsorption on New and Modified Inorganic Sorbents, Stud. Surf. Sci. Catal., 99 (1996) 93.
[23] R.S.A. de Lange, K. Keizer, A.J. Burggraaf, Characterisation of microporous non-supported membrane top layers using physisorption techniques, J. Porous Mater. 1 (1995) 139.
[24] W.J. Koros, Y.H. Ma, T. Shimidzu, Terminology for membranes and membrane processes, Pure Appl. Chem. 68 (1996) 1479.
[25] V. Raman, O.P. Bahl, N.K. Jha, Synthesis of silicon oxycarbide through the sol–gel process, J. Mater. Sci. Lett. 12 (1993) 1188.
[26] E.F. Vansant, P. Van der Voort, K.C. Vrancken, Characterisation and chemical modification of the silica surface, in B. Delmon, J.T. Yates (Eds.), Stud. Surf. Sci. Catal., 93 (1995) 59.
[27] S. Storck, H. Bretinger, W.F. Maier, Characterization of micro- and mesoporous solids by physisorption methods and pore size analysis, Appl. Catal., A, 174 (1998) 137.
[28] G. Horváth, K. Kawazoe, Method for the calculation of effective pore size distribution in molecular sieve carbon, J. Chem. Eng. Jpn. 16 (1983) 470.
[29] S.J. Gregg, K.S.W. Sing, Adsorption, Surface Area and Porosity, second edn., Academic Press, New York, 1982.